INSTITUTE OF PHYSICS PUBLISHING SUPERCONDUCTOR SCIENCE AND TECHNOLOGY

Supercond. Sci. Technol. **14** (2001) 16–29 www.iop.org/Journals/su PII: S0953-2048(01)17021-1

Critical currents in Josephson junctions with macroscopic defects

N Stefanakis and N Flytzanis

Department of Physics, University of Crete, PO Box 2208, GR-71003, Heraklion, Crete, Greece

Received 11 September 2000

Abstract

The critical current in Josephson junctions of conventional superconductors with macroscopic defects is calculated for different defect critical current densities as a function of the magnetic field. We also study the evolution of the different modes with the defect position, at zero external field. We study the stability of the solutions and derive simple arguments, that could help the defect characterization. In most cases a re-entrant behaviour is seen, where both a maximum and a minimum current exist.

(Some figures in this article are in colour only in the electronic version; see `www.iop.org`)

1. Introduction

The interaction of localized magnetic flux (fluxons) with defects (natural or artificial) or impurities in superconductors or junctions has important effects on the properties of bulk superconductors or the behaviour of Josephson junctions, respectively [1]. The flux trapping from defects, which is of major importance in Josephson junctions [2], can modify the properties of polycrystalline materials with physical dislocations, for example grain boundary junctions [3]. In this category one can also consider grain boundary junctions in $YBa_2Cu_3O_7$ [4] where the tunnelling current is a strongly varying function along the boundary. This strong inhomogeneity makes them good candidates for SQUID-type structures [5]. Phenomenologically the current–voltage (I–V) characteristics of grain boundary junctions are well described [6] by the resistively shunted junction model [7]. The grain boundary lines often tend to curve, while the junction is very inhomogeneous and contains non-superconducting impurities and facets of different length scales [8, 9]. The linear increase in the critical current with length in grain boundary junctions of high-T_c superconductors, which is a different behaviour from the saturation of the inline geometry of a perfect junction, can be explained by the presence of impurities [10]. Therefore it is interesting to study flux trapping in impurities, especially when it can be controlled. Modern fabrication techniques can, with relative ease, engineer any defect configuration in an extremely controlled way.

In bulk materials there are several types of defects that can influence the critical current in high-temperature superconductors, such as $YBa_2Cu_3O_x$ type materials. They include 3D inclusions, 2D grain boundaries and twin boundaries, and point defects such as dopant substitutions or oxygen vacancies [1]. For example, the homogeneous precipitation of fine Y_2BaCuO_5 non-superconducting particles in the melt processing of $YBa_2Cu_3O_x$ leads to high J_c values due to particle pinning centres [11]. Similar behaviour is observed in $NdBa_2Cu_3O_x$ bulk crystals with $Nd_4Ba_2Cu_2O_{10}$ particles [12]. The case of the peak effect in twin-free Y123 with oxygen deficiency is also of interest. In this case, one sees a linear increase (peak effect) of the critical current at small magnetic fields, when growth is under oxygen reduction [13]. For the fully oxidized crystal one expects a decrease. The peak effect is attributed to flux trapping. Information on the defect density and activation energies can also be obtained from the I–V characteristics, as was the case for several types of defects which were also compared to Au^+ irradiated samples with artificial columnar defects [14]. These columnar defects also act to trap flux lines in an YBCO film, which is considered as a network of intergrain Josephson junctions modulated by the defects. In this case, assuming a distribution of contact lengths, one finds a plateau in the curve of the critical current density against the logarithm of the field [15].

The study of the long size of impurities is going to give information beyond the theories which concern the small amplitude of inhomogeneities [16]. Also, it is possible to directly compare the numerical results with experiments in long junctions obtained with electron beam lithography [17]. This is a powerful technique which allows the preparation and control of arrays of pinning centres. Another method is ionic irradiation, which produces a particular kind of disordered array, consisting of nanosized columnar defects [14, 18]. The variation of the critical current density can also occur due to temperature gradients [19].

The activity in an area of high critical current densities in the presence of a magnetic field is hampered by defects

due to the difficulty of having a high quality junction with a very thin intermediate layer. Thus significant activity has been devoted to this area, since, for example, the energy resolution of the SQUID [20] and the maximum operating frequency of the single-flux quantum logic circuit [21], to name two applications, depend, respectively, inversely and directly on the plasma frequency ω_p, with $\omega_p \sim J_c^{1/2}$. The fundamental response frequency of Josephson devices, the Josephson frequency ω_J, also depends on the critical current density. On the other hand, a drawback is that high critical current densities lead to large subgap leakage currents [22] and junction characteristics degrade rapidly with increasing J_c.

Variations in the critical current density also influence the I–V characteristics introducing steps under the influence of both a static bias current and irradiation with microwaves [23]. In that case the variation is quite smooth (of sech type), so that the fluxon and its motion can be described by a small number of collective coordinates. Interesting behaviour is also seen in both the static and dynamic properties for the case of a spatially modulated J_c with the existence of 'supersoliton' excitations [24, 25] and the case of columnar defects [26, 27] or disordered defects [10].

The trapping of fluxons can be seen in the $I_{max}(H)$ curves where we also expect important hysteresis phenomena when scanning the external magnetic field. The hysteresis can be due to two reasons: (i) one is due to the non-monotonic relation between the flux and the external magnetic field [28] arising from the induced internal currents, and (ii) the other is from the trapping or detrapping of fluxons by defects. The effect of a defect on a fluxon and the strength of the depinning field depends strongly in the size of the defect, the type of defect and the position of the defect. Here we will consider the case where the widths of the defects is of the order of the Josephson penetration depth. In this range we expect the strongest coupling to be between fluxons and defects. We will also consider the case of a few defects in the low magnetic field region where pinning and coercive effects are important.

The organization of the paper is as follows. In section 2 the sine-Gordon model for a Josephson junction is presented. In section 3 we present the results of the critical current I_{max} against the magnetic field of a junction with an asymmetrically positioned defect. The variation of the I_{max} and the flux content, N_f, with the defect critical current density and position are presented in sections 4 and 5, respectively. The effect of multiple pinning centres is examined in sections 6 and 7. In section 8 we examine a defect with a smooth variation of the critical current density. In the last section we summarize our results.

2. The junction geometry

The electrodynamics of a long Josephson junction is characterized from the phase difference $\phi(x)$ of the order parameter in the two superconducting regions. The spatial variation of $\phi(x)$ induces a local magnetic field given by the expression

$$\mathcal{H}(x) = \frac{\mathrm{d}\phi(x)}{\mathrm{d}x} \tag{1}$$

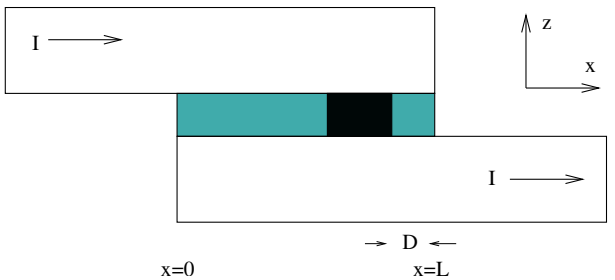

Figure 1. The geometry of the junction. The dark shaded region marks the defect in the intermediate layer. ℓ is the junction length and D is the separation between the left-hand edges of the defect and the junction.

in units of $H_0 = \Phi_0/(2\pi d\lambda_J)$ where Φ_0 is the quantum of flux, d is the magnetic thickness and λ_J is the Josephson penetration depth. The magnetic thickness is given by $d = 2\lambda_L + t$ where λ_L is the London penetration depth in the two superconductors and t is the oxide layer thickness. The λ_J is also taken as the unit of length. The current transport across the junction is taken to be along the z-direction. We describe a 1D junction (shown in figure 1) with width w (normalized to λ_J) in the y-direction, small compared to unity. The normalized length in the x-direction is ℓ. The superconducting phase difference $\phi(x)$ across the defected junction is then the solution of the sine-Gordon equation

$$\frac{\mathrm{d}^2\phi(x)}{\mathrm{d}x^2} = \tilde{J}_c(x)\sin[\phi(x)] \tag{2}$$

with the inline boundary condition

$$\left.\frac{\mathrm{d}\phi}{\mathrm{d}x}\right|_{x=\pm\ell/2} = \pm\frac{I}{2} + H \tag{3}$$

where I and H are the normalized bias current and external magnetic field. $\tilde{J}_c(x)$ is the local critical current density, which is $\tilde{J}_c = 1$ in the homogeneous part of the junction and $\tilde{J}_c = j_d$ in the defect. Thus the spatially varying critical current density is normalized to its value in the undefective part of the junction J_0 and the λ_J used above is given by

$$\lambda_J = \sqrt{\frac{\Phi_0}{2\pi\mu_0 d J_0}}$$

where μ_0 is the free space magnetic permeability. One can also define a spatially-dependent Josephson penetration depth by introducing $\tilde{J}_c(x)$ instead of J_0. This is a more useful quantity in the case of weak distributed defects.

In the case of overlap boundary conditions equations (2) and (3) are modified:

$$\frac{\mathrm{d}^2\phi(x)}{\mathrm{d}x^2} = \tilde{J}_c(x)\sin[\phi(x)] - I \tag{4}$$

and

$$\left.\frac{\mathrm{d}\phi}{\mathrm{d}x}\right|_{x=\pm\ell/2} = H. \tag{5}$$

We can classify the different solutions obtained from (2) with their magnetic flux content

$$N_f = \frac{1}{2\pi}(\phi_R - \phi_L) \tag{6}$$

in units of Φ_0, where $\phi_{R(L)}$ is the value of $\phi(x)$ at the right(left)-hand edge of the junction. Knowing the magnetic flux one can also obtain the magnetization from

$$M = \frac{2\pi}{\ell} N_f - H. \tag{7}$$

For a perfect junction, a quantity of interest is the critical magnetic field for flux penetration from the edges, denoted by H_{c1}. For a long junction it is equal to two, while for a short junction it depends on the junction length. Due to the existence of a defect this value can be modified, since we have the possibility of trapping at defects. For a short junction we have penetration of the external field in the junction length, so that the magnetization approaches zero. For a long junction it is a non-monotonic function of the external field H.

To check the stability we consider small perturbations $u(x,t) = v(x)\,\mathrm{e}^{st}$ on the static solution $\phi(x)$, and linearize the time-dependent sine-Gordon equation to obtain

$$\frac{\mathrm{d}^2 v(x)}{\mathrm{d}x^2} - \tilde{J}_c(x)\cos\phi(x)v(x) = \lambda v(x) \tag{8}$$

under the boundary conditions

$$\left.\frac{\mathrm{d}v(x)}{\mathrm{d}x}\right|_{x=\pm\ell/2} = 0$$

where $\lambda = -s^2$. It is seen that if the eigenvalue equation has a negative eigenvalue, the static solution $\phi(x)$ is unstable. There is considerable eigenvalue crossing so that we must monitor several low eigenvalues. This is especially true near the onset of instabilities.

3. Asymmetric defect

In the following we will consider the variation of the maximum critical current as a function of the magnetic field for several defect structures. We start with a long ($L > \lambda_J$) junction of normalized length $\ell = 10$ with a defect of length $d = 2$ which is placed $D = 1.4$ from the right-hand edge. Thus the defect is of the order of λ_J. We plot in figure 2(a) the maximum critical current I_{max} variation with the magnetic field. The different curves correspond to phase distributions for which we have a maximum current at a given value of the magnetic field H. The overlapping curves, called modes, have different flux content as seen in figure 2(b) where we plot the magnetic flux in units of Φ_0 for zero current against the external field. The magnetic flux is only a weak function of the external current.

For the perfect junction there is no overlap in the magnetic flux between the different modes. In fact, each mode has a flux content between $n\Phi_0$ and $(n+1)\Phi_0$ and is therefore labelled the $(n, n+1)$ mode [28]. Here, in the case of the defect, the range (at zero current) of flux for each mode can be quite different and the labelling is with a single index $n = 0, 1, 2, \ldots$ corresponding, in several cases, to the (0, 1), (1, 2), (2, 3), ... modes of the perfect junction. There are, in several cases, several modes with similar fluxes. To distinguish them we add a letter following the index n.

The maximum I_{max} is obtained for mode 1 and the increase comes from the trapping of flux by the defect. We have to note that the (d, e) part of this mode is a continuation of the (a, b) part of mode 0. In both cases we have an entrance of the flux from the defect-free part of the junction and the instability in the critical current occurs when $\phi(-\ell/2) = \pi$. Here, and in the following, we will take this to mean equal to π modulo 2π. For the maximum current (at $H < 0$) the equation is $H - I/2 = -2$. This can be understood from the pendulum phase diagram, where the $\phi_x = -2$ is the extremum slope, and thus the relation $I_{max} = 4 + 2H$ holds. For the (b, c) part of

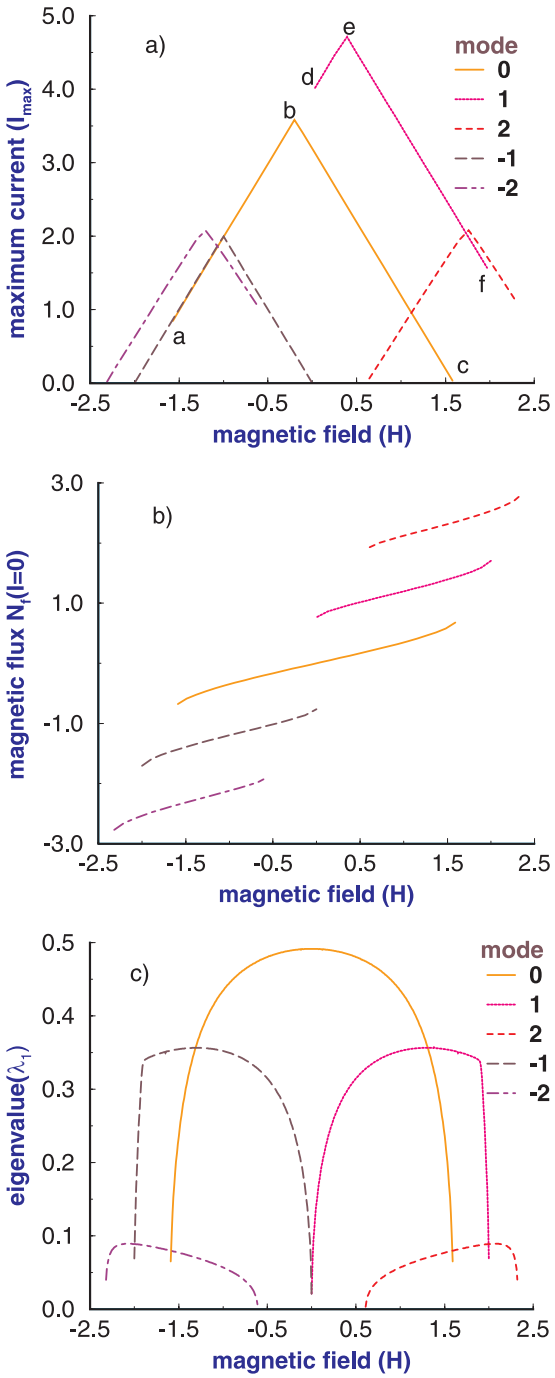

Figure 2. (a) Critical current I_{max} and (b) magnetic flux at zero current plotted against the magnetic field H, for the different modes; $\ell = 10$ and $D = 1.4$. (c) The evolution of the lowest eigenvalue λ_1 with the external field for the different modes. At the extremes of each mode λ_1 vanishes.

mode 0 the flux enters from the right, where the defect is. This reduces the critical current compared to the perfect junction 0 mode [28, 29]. Note that the 0 mode has its critical current I_{max} peak slightly to the left of $H = 0$ in the I_{max} against H diagram, and to the left of $N_f = 0$ in an I_{max} against N_f diagram (see figure 11(a) below). Also, in the absence of current, reversing the direction of H only changes the sign of the slope $\mathrm{d}\phi/\mathrm{d}x$, but the phase difference (in absolute values) at the two ends will be the same. Thus the zero mode at $I = 0$ extends for $-1.6 \leqslant H \leqslant 1.6$. This is not clearly seen due to curve overlapping in the left-hand side. Comparing the I_{max} for the modes 1 and -1 we see that $I_{max}(1) > I_{max}(-1)$. In both cases a fluxon (or antifluxon) is trapped in the defect. The major difference in the I_{max} comes mainly from the phase distribution which in the mode 1 case leads to a large positive net current in the defect-free side, while in the -1 mode the net current in the defect-free side is very small.

For the mode 1, at $H \approx 0$ and zero current the instability happens due to the competition of the slope of the phase at the defect centre and at the right-hand edge, while at the other end at $H = 2$, the field at the defect centre becomes equal to the external field applied at the boundaries and there is no such competition. In this case the instability sets in due to the critical value of the phase at the defect-free boundary (i.e. $\phi_x(-\ell/2) = 2$). The situation is analogous for mode -1. For $H \approx 0$ the instability sets in due to the depinning of the antifluxon while for $H = -2$ this is due to the critical value of the phase at the defect-free part of the junction. For mode 0 we have no fluxon trapping at the defect, even though the instability at the two extremes with $H = \pm 1.6$ at zero current is caused by the tendency to trap a fluxon or antifluxon, respectively, at the defect. At higher values of the magnetic field ($|H| > 1.6$) we have stability for a range of non-vanishing current values as will be discussed below. Thus this value can be considered as the minimum value for the introduction of fluxons in the junction. Let us remark that for the perfect junction, or a junction with a centred defect, the corresponding values for fluxon introduction would be equal to two. Thus there is a decrease of the critical field as the defect moves away from the centre. For the 0 mode a centred defect would have no influence on the solution.

The results for the maximum current are in agreement with the stability analysis. In figure 2(c) we present the lowest eigenvalue λ_1 for the different modes in a zero external current, $I = 0$, as a function of the magnetic field H. The sudden change in slope for the modes -1 and 1 is because at that point a new eigenvalue becomes lower. The λ_1 is positive denoting stability and becomes zero at the critical value of the magnetic field, where a mode terminates. The symmetry about zero magnetic field is due to the symmetric boundary conditions for $I = 0$. The change of the sign of H changes the sign of the phase distribution, but the $\cos\phi$ in (8) remains unchanged. This symmetry is lost when a finite current is also applied. Also, there are solutions (not presented in the figure) for which the stability analysis gives negative eigenvalues, i.e. instability. These solutions may be stabilized when we insert multiple impurities.

In figure 3(a) we specifically draw only the 1 mode, to be discussed in more detail. Here we changed the procedure in searching for the maximum current. Up to now we followed

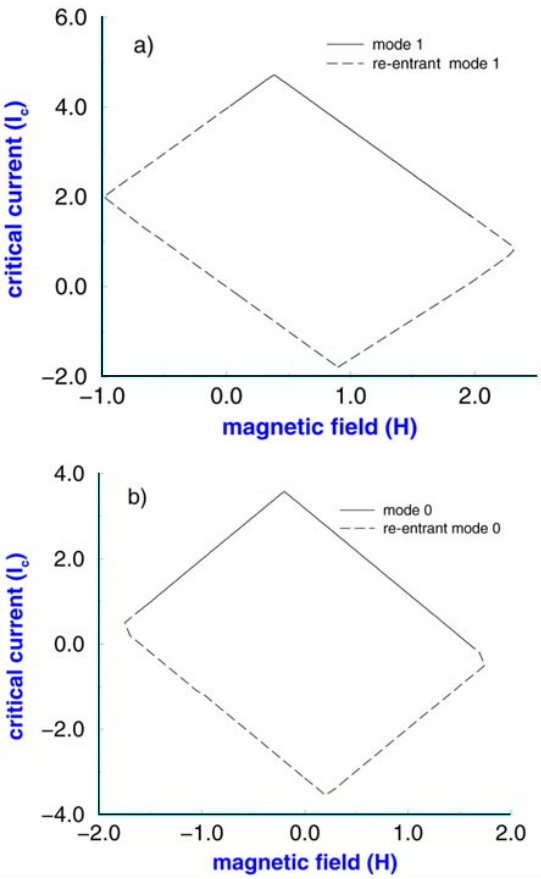

Figure 3. (a) Critical values of the bias current as a function of the magnetic field. The full curve is drawn for mode 1 obtained with the usual procedure starting form zero current and increasing the current to the critical value, while the broken curve represents the values obtained with the re-entrant procedure described in the text. (b) The same as in (a), but for mode 0.

the standard experimental procedure, i.e. we scan the magnetic field and for each value of H we increase the current I, starting from $I = 0$, until we reach the maximum current. Here we consider the possibility that for $I > 0$ there is also a lower bound in the value of the current for some values of the magnetic field. This requires a search where we vary both H and I simultaneously. Thus we see that for $H < 0$ there is a lower bound, given approximately by the line $H + I/2 \approx H_{cl}$ where $H_{cl} \approx 0$ is the critical value of H at $I = 0$, for which we have depinning of the trapped fluxon. Over this curve the slope ϕ_x at the right end (near defect) is kept constant and equal to H_{cl} and above this line the fluxon remains pinned and it should be stable. This line ends at $H = -1$, since in that case the extremum value $\phi_x = -2$ is reached at the left end. Increasing now in that range of H the bias current we find that also the upper bound of the bias current versus the magnetic field curve, obtained with the standard procedure (full curve), extends further to the left. The equation for this line is approximately given by $H - I/2 = -2$, with an extremum at $\phi_x(-\ell/2) = -2$. Thus the instability on this line arises from the left side (far from the defect). It extends up to $H = -1$ for a long junction and joins the other line $H + I/2 = H_{cl}$.

The above calculations were performed for a long junction so that the fields at the two ends do not interfere. For shorter

lengths, however, the two ends feel each other and in such a case the two instabilities are not independent. This means that the tail of the defect-free side field will compete with the slope of the trapped field. Then the two lines, $H + I/2 = H_{cl}$ and $H - I/2 = -2$, end before they meet (at $H \approx -1$) at a cut-off magnetic field. Also, for short junctions we expect that the lines have some curvature. A similar discussion holds for the right end of the 1 mode. Again there is a lower current (positive) bound given by $H - I/2 = 2$ due to the instability at the left end ($\phi_x(-\ell/2) = 2$), and an upper bound given by $H + I/2 = H_{cr}$, where $H_{cr} \approx 2.8$, due to fluxon depinning. On the same diagram, we show the lower bound for negative currents. Thus we see that there is strong asymmetry for positive and negative currents. We remark that for negative currents, mode 1 is very similar to mode (1, 2) with no defect [28]. This is because the right-hand boundary is determined by an instability at the defect-free side. The left-hand boundary is again very close because $H_{cl} \approx 0$. So an interesting effect of the defect is that we have this strong asymmetry for positive and negative currents.

We would obtain a similar picture if we considered the -1 mode. In fact we obtain the same curves (as for mode 1) if we put $I \to -I$ and $H \to -H$. This is consistent with the -1 mode shown in figure 2(a). The discussion can also be extended to the other modes. In figure 3(b) we show the result of a similar scan for the 0 mode, but for the sake of brevity we will not discuss the -1, -2 and 2 modes. In any case, when the number of fluxons increases one must rely on numerical calculations rather than simple arguments.

4. Variation with the defect critical current

In the previous section we considered the case of a microresistance defect. With present-day masking techniques we can also consider any finite critical current (lower or higher) in the defect. This situation very often arises in junctions with high critical current densities, where small variations in the thickness can create strong critical current density variations. Thus for the previous asymmetric defect configurations we will study the effect of the defect critical current density in the magnetic interference pattern $I_{max}(H)$. We will concentrate on the 0 and 1 modes.

(i) *Mode 0.* In figure 4 we see the $I_{max}(H)$ variation for mode 0 for decreasing values of the defect critical current density from $j_d = 2$ to $j_d = 0$. Let us discuss first the case for $j_d \leqslant 1$. For the perfect junction, where $j_d = 1$, we have a symmetric distribution about $H = 0$. As we decrease j_d the flux content of this mode (and the extremum H) is symmetrically reduced (see figure 2(b)). It is not apparent from the figure, due to the superposition of several curves on the left-hand side of the diagram, but as expected the range of the magnetic field is symmetric about $H = 0$ at zero current. The corresponding $I_{max}(H)$ curves, however, are not symmetric. The right-hand side of the curves is displaced towards smaller critical fields with decreasing j_d. This means that the critical field at $I = 0$ required to introduce a fluxon from the ends decreases due to the existence of the defect, which acts with an attractive force on the fluxon. The curves are linear and can be approximated by the equation $I(H) = 4 - 2(H + \delta H_c)$, where δH_c is the decrease in the critical field H_{c0} and depends

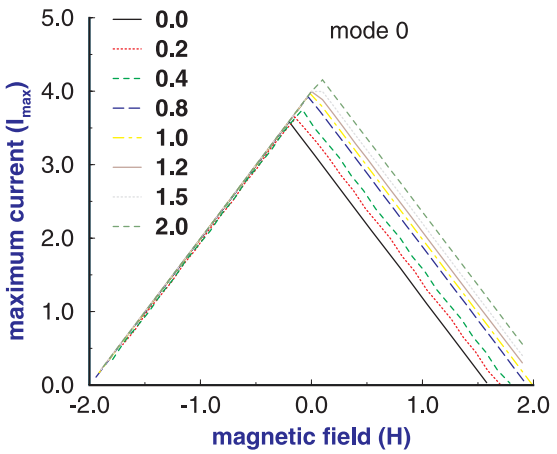

Figure 4. Critical current as a function of the magnetic field, for mode 0, for different values of the defect critical current density j_d.

on j_d. A similar decrease happens for negative magnetic fields where the defect tries to pin an antifluxon. Even for higher currents the right-hand side critical field is determined by the tendency of the defect to attract a fluxon. The left-hand side, however, remains rigid (but is shifted along the line). This is due to the entrance of magnetic flux from that part of the junction where there is no defect. The instability in the critical current occurs when $\phi(-\ell/2) = \pi$ for every value of j_d. From the pendulum phase diagram, which is the classical analogue of the Josephson junction, the extremum occurs at $\partial_x\phi(-\ell/2) = -2$, or $H - I/2 = -2$, which is the equation for this triangular side. At near zero current the critical field is influenced by the attractive action of the defect. At low currents and extreme negative magnetic fields the I_{max} curve shows a re-entrance behaviour so that it is not stable at low and high currents, but only for a finite intermediate range of current values. This way we reconcile the different origins of the instability mechanisms $\phi(-l/2) = \pi$ at high currents and the defect influence discussed for the right-hand side of the mode.

For $j_d > 1$ we see an increase in the I_{max}, while the critical magnetic field at $I = 0$ remains almost constant at about $H_{cr} \approx 1.9$. The instability at that point is due to the trapping of flux in the region between the positive defect and the right-hand edge of the junction. The field for this is expected to be near $H = 2$ if the right-hand defect-free part is of a length of the order of the Josephson length. Thus it is the same value for flux penetration from the perfect junction edges. It will vary weakly with j_d.

(ii) *Mode 1.* Mode 1 in the perfect junction has a full fluxon for a magnetic field $H = 0.07$. The phase distribution is about $\theta = \pi$ where the energy has a minimum. At the end of this mode at $H = 2.07$, where two fluxons have entered the junction, the phase changes from $\phi(-\ell/2) = -\pi$ to $\phi(\ell/2) = 3\pi$. When the defect is inserted this mode is significantly modified due to the flux trapping in the defect.

In figure 5 we see the magnetic interference pattern for this mode for different values of the defect critical current density. For $0 < j_d < 0.7$ the I_{max} against H curves are displaced downwards, and a fluxon is trapped in the defect. We notice that all the curves for $j_d < 0.7$ have the same critical magnetic field $H = 2$ for $I = 0$. This is because, at this end of the

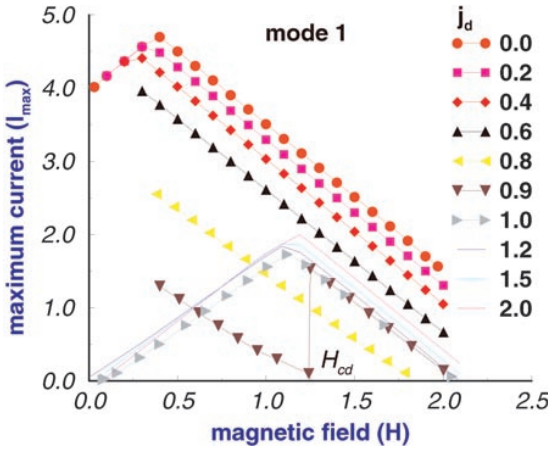

Figure 5. Same as in figure 4, but for mode 1.

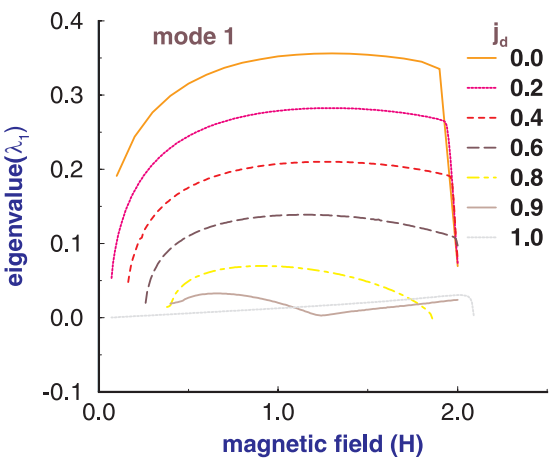

Figure 6. The lowest eigenvalue plotted against the magnetic field for mode 1 for different values of the defect critical current density j_d.

mode, at $I = 0$ the instability arises at the side with no defect where the phase reaches the critical value $\phi = \pi$ (modulo 2π). Of course, as discussed in the previous section, we have a re-entrant behaviour above $H = 2$. At the other end, for a small magnetic field the instability is due to the depinning of the trapped fluxon. For $0.7 < j_d \leqslant 1.0$ the defect can trap the flux only for $H < H_{cd}$, where the value of the H_{cd} depends on the defect critical current j_d; in figure 5 it is shown for $j_d = 0.9$. Notice that for this value of j_d the fluxon is very weakly trapped, and the untrapping process happens slowly over a range of magnetic field values. For $H > H_{cd}$ the fluxon has moved away from the defect, and for this weak defect the junction does not feel it. The critical current goes abruptly close to the curve for the perfect junction. We conclude that the behaviour of the junction for values of j_d close to $j_d = 1$ is determined by the ability of the defect to trap one fluxon. This can also be seen from the change in the lowest eigenvalue variation with the external field H, at values of the critical density $j_d > 0.7$, in figure 6.

For $j_d > 1$ (fine lines in figure 5) the $I_{max}(H)$ curve has a similar form as for $j_d = 1$, i.e. there is no fluxon trapping. Again, as in the 0 mode, the H_{cr} at $I = 0$ stays around 2.0 and is again due to the trapping of flux in the right-hand edge.

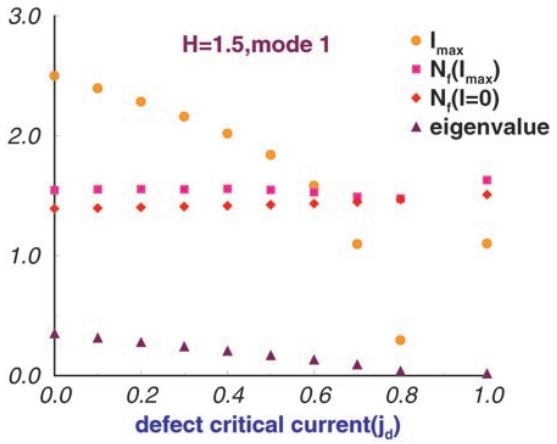

Figure 7. Critical current plotted against the defect critical current density j_d, for a magnetic field equal to $H = 1.5$ and for mode 1. In the same figure the magnetic flux at zero and maximum current and the lowest eigenvalue at $I = 0$ are plotted as a function of j_d.

In figure 7 we present the evolution of I_{max} with the defect critical current density j_d for a magnetic field $H = 1.5$. For this value of the magnetic field there are no solutions with trapped fluxons for $j_d > 0.83$. The lowest eigenvalue at $I = 0$ becomes zero at this point. For $j_d > 0.83$ and $H > 1.5$ there are solutions which are not trapped. For these solutions the maximum current coincides with that of the perfect junction and there is a discontinuity in the curves. Notice the point at $j_d = 1.0$. In the same figure we also show the magnetic flux at $I = 0$ and at I_{max}, which is almost constant as a function of j_d as expected, with a small difference between the two different current curves.

5. Variation with the defect position

In figure 8(a) we see the evolution of the critical current at zero magnetic field as we move the defect from the right-hand edge of the junction, $D = 0$, to the left-hand edge, $D = 8$. The position is measured from the edge of the junction to the nearest edge of the defect. We examine the several modes separately.

(i) *Mode 0.* For this mode and for $I = 0$, we are able to find solutions for all the defect positions. As we can see in figure 8(b), the corresponding magnetic flux at I_{max} is slowly changing and equal to zero when the defect is in the junction centre; but when the defect is placed close to the ends the magnetic flux at the maximum current deviates from zero. The critical current for this mode is symmetric for defect positions about the junction centre, and has its maximum value when the defect is at the centre. This is because at that position it does not influence the solution at the edges, which is very close to the defect-free case, while near the centre the phase is almost zero. However, when the defect comes close to the junction ends the defect cuts into the area in which the current flows, and the critical current is reduced.

For even smaller distances, $D = 0.2$ and $D = 0$, there is a jump to solutions which correspond to a current which is much higher than that of the 0 mode for nearby D values. This is because the defect cuts negative current regions and for this position we have an increase of the critical current. In

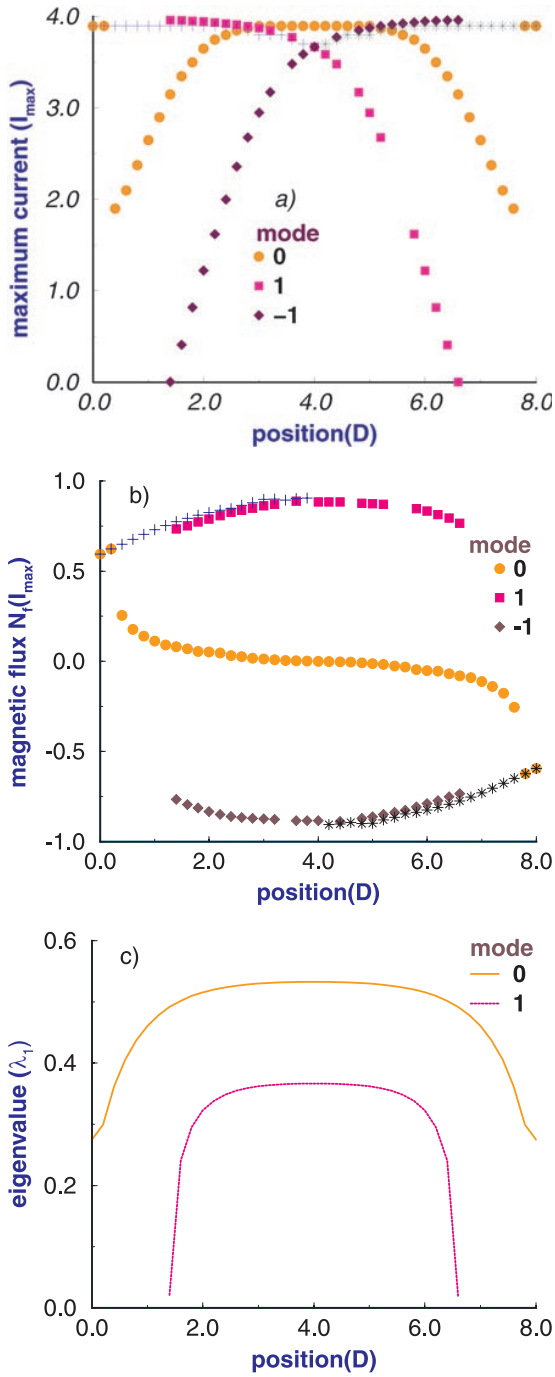

Figure 8. The variation of (a) the maximum current I_{max} and (b) the magnetic flux N_f at the maximum current plotted against the defect position, D, measured from the right-hand edge of the junction, for modes 0, 1, -1. The crosses and stars are continuations of the two points at the two ends of the graph. (c) The corresponding lowest eigenvalue at zero current plotted against the defect position, D, for modes 0, 1. The -1 mode eigenvalue is the same as for the 1 mode.

fact, these solutions (see the + symbols in figure 8(a)) are very close to the solutions of a perfect junction within the defect-free area, except that now the defect at the edge can give a contribution to the flux, but no contribution to the current. Thus the flux is much higher than that of the 0 mode and it approaches that of mode 1. Nevertheless, these points should be considered as a separate mode. In fact they are part of a branch (crosses). At these distances there are no other modes for $H = 0$. Similar results were obtained by Chow *et al* [30] where they attributed this enhancement in the I_{max} for small distances to a self-field which was generated by the current, penetrating into the defect and resisted any further penetration of field. To overcome this resistance it was necessary to apply a higher current. However, they do not distinguish between modes with different flux content, and their evolution with the defect position.

(ii) *Modes 1, −1.* For these modes we do not have solutions for all the defect positions at $I = 0$ and $H = 0$, but only in the range $1.4 < D < 6.6$, as seen in figure 8(c), where the lowest eigenvalue is plotted as a function of the defect position for the different modes. The curves for the 1 and -1 modes coincide, while the 0 mode shows a change of slope corresponding to the last two points ($D = 0$ and 0.2 discussed above) which belong to another curve. Mode -1 has a trapped antifluxon in the defect. When the defect is to the left ($4.0 < D < 6.5$), then the instability in the current of mode -1 at $H = 0$ is created at the right end of the junction when the phase reaches the critical value $\phi(l/2) = \pi$. This instability occurs for currents which are less than those necessary to unpin the antifluxon. Notice that on increasing the current there is no competition with the slope of the antifluxon trapped in the left end. Thus at this point (for $4.0 < D < 6.5$) the maximum current is very close to the defect-free junction mode 0, except that in this case $N_f \approx -1$ is close to an antifluxon. At the other end ($D < 4.0$) the instability for mode -1 is caused by the depinning action of the applied current, which now takes much smaller values (close to zero) because of competition with the pinned fluxon. The phase distribution at the defect-free end is that expected for $H = 0$ and I close to zero. Mode 1 with a trapped fluxon has a reflection symmetry (about the centre) in the I_{max} against D curve and the instability for $D > 4.0$ occurs at the left end of the junction, which is the opposite case to mode -1. The eigenvalue becomes zero at the positions $D = 1.4$ and $D = 6.6$. The $\lambda_1(D)$ curve coincides with modes 1 and -1 due to the fact that the phase distributions for the same D for these modes are symmetric about $x = L/2$, and the $\cos\phi(x)$ that enters the eigenvalue equation is the same.

In the remainder of this paper we examine the variation of the critical value at which the instability sets in, as we scan the magnetic field in the positive (negative) direction $H_{cr}(H_{cl})$ for zero current, for the different modes, as a function of defect position. This instability can be attributed to the pinning or depinning field or to the critical value of $\mathrm{d}\phi/\mathrm{d}x$ at the defect-free edge, depending on the particular mode that we are considering. Explicitly, for the mode 0 the instability in the $H_{cl}(H_{cr})$ is due to the pinning of a fluxon (antifluxon). In this mode the defect has no influence for positions close to the centre, as seen in figures 9(a) and 9(b). However, as we move the defect close to the edges the pinning field $H_{cl}(H_{cr})$ is reduced in absolute value because it is easier to trap a fluxon (antifluxon). For mode 1, the H_{cr} is constant for all defect positions. This is due to the fact that at $I = 0$ it is the phase distribution at the defect-free edge of the junction that determines the instability. Notice that due to the re-entrant character the critical magnetic field takes higher values at larger bias currents, which vary with defect position. The H_{cl} curve depends on the phase distribution near the defect and therefore

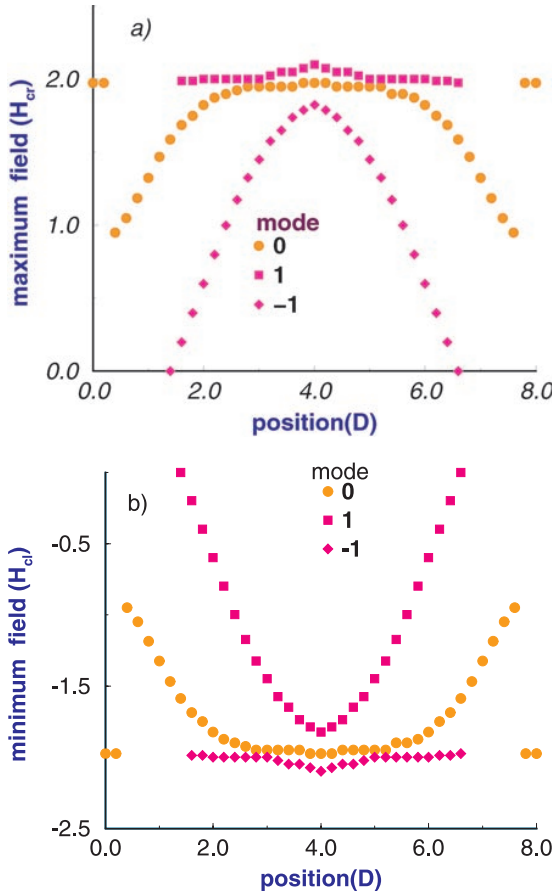

Figure 9. (a) The critical value of the instability as we scan the magnetic field to the right H_{cr} as a function of the defect position D, for the modes 0, 1, -1. (b) The same as (a) but to the left, for the H_{cl}.

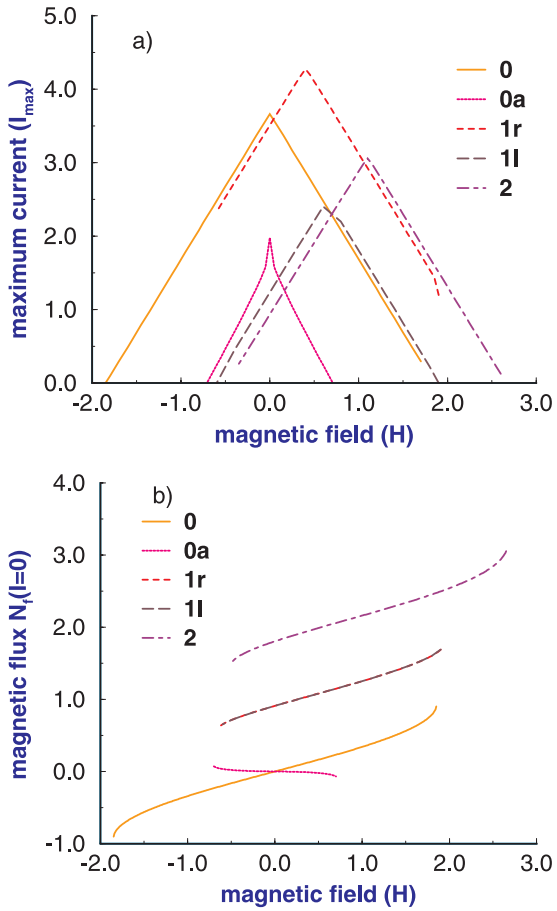

Figure 10. (a) Critical current I_{max} and (b) magnetic flux N_f plotted against the magnetic field H, for the different modes and for a junction of length $\ell = 10$, which contains two symmetric pinning centres of length $d = 2$.

is strongly defect position dependent. For mode -1, the picture is reversed compared with the 1 mode. In this case the H_{cl} is constant while the H_{cr} varies with position. Note that in this mode the depinning of an antifluxon is the reason that causes the instability at H_{cr}.

6. Two symmetric pinning centres

As noted, defects (with $j_d < 1$) or inhomogeneities in the junction can play the role of pinning centres for a fluxon. In this section we discuss more precisely the effect of multiple pinning centres on the magnetic interference patterns $I_{max}(H)$ and the flux distribution. The pinning effect of the Josephson junction has also been analysed in [31, 32], by using a simple mechanical analogue. The analogies of the mixed state of type II superconductors and the vortex state of the Josephson junction were discussed in these references. In figure 10(a) we present, as an example, the critical current I_{max} plotted against the magnetic field for a junction which contains two defects of length $d = 2$ placed symmetrically at a distance $D = 2$ from the junction's edges. We examine the following modes grouped according to flux content.

(i) *Modes 0, 0a.* These modes have magnetic flux antisymmetrical around zero field, as seen from figure 10(b) where the magnetic flux is plotted against the magnetic field. At $I = 0$ and magnetic field $H = -0.7$, the $0a$ mode contains one fluxon trapped in the left-hand defect, while an antifluxon exists at the other part of the junction. As H increases towards 0.7 the picture changes slowly, so that the antifluxon is pinned in the right-hand defect. The stability analysis shows that this mode is unstable. We remark that there are also other unstable modes near zero flux, which we will not present here. For example, there is another unstable mode with the same flux as $0a$, but a much higher critical current (the same as the 0 mode). Mode 0 has phase distributions which are similar to the corresponding mode of the homogeneous junction since it has no trapped flux in each defect.

(ii) *Modes 1l, 1r.* These modes have magnetic flux close to unity, and are both stable. For mode $1r$ one fluxon has been trapped in the right-hand defect, and in mode $1l$ the vortex is trapped in the left-hand defect. Due to the symmetry this mode has the same magnetization as mode $1r$, but the critical current is reduced. The phase distributions for modes $1r$ and $1l$ at zero current are related by $\phi_{1l}(x) = 2\pi - \phi_{1r}(-x)$. The maximum field, $H = 1.9$ (at $I = 0$), for both modes is determined by an instability at the fluxon-free side. At the other extreme there is a competition at the fluxon side between the applied field and the field created by the pinned fluxon. Thus the critical field at $H = -0.62$ can be considered as a coercive field and below this value the fluxon is unpinned. The two modes have

characteristically different currents and this depends on the current through the fluxon-free defect, since the pinned fluxon itself gives no major contribution. Thus the maximum current is much larger for the $1r$ mode. The opposite would be true if we look for negative currents. There are also symmetrically situated modes that correspond to an antifluxon in the left-hand or right-hand defects, which are not shown in figure 10(a). The respective flux is antisymmetric with H around $H = 0$.

In figure 10(a) we also show mode 2 with flux around two fluxons. Several unstable modes are not shown, for the sake of clarity. Their analysis, however, can show the connection between different modes, while a defect in the correct place with proper characteristics can stabilize these solutions. We conclude that depending on the positions where the vortex is trapped we may have modes with the same magnetic flux content, but different critical currents. Also, due to soliton localization on the defects, we may have stable states with magnetic flux close to unity, for zero magnetic field. These states together with the one existing in the homogeneous junction form a collection of stable states in a large H interval. We must comment here that states with unit flux, for zero magnetic field ($H = 0$), exist in the homogeneous junction as a continuation of the stable 1 mode to negative magnetic fields, but, as we found in a previous work [28], are unstable. So we may argue here that the presence of defects stabilizes these states.

In comparing the results for one (figure 2(a)) and two defects (figure 10(a)) we see some similarities and differences. In the case of two defects new modes appear, but, also, the region of stability of the equivalent modes is different. This is more clearly seen in figure 11 where we plot I_{max} against N_f for both cases. This presentation is useful since N_f is a nonlinear function of H. This plot (figure 11(a)) is a combination of figures 2(a) and 2(b). We should point out that the maximum peak in the current in both cases is due to the trapping of a fluxon in the defect at the right-hand side. The maximum of the 0 mode is very close in both cases and this happens because this mode does not involve fluxon trapping. The $1r$ mode for the two-defect case is very close to the 1 mode of the single-defect case, since in both cases there is a fluxon trapped on the same side. In the two-defect case we see an enlargement of the region of stability, so that the modes overlap. The thin continuation lines in modes 0 and 1 for the single defect are in the re-entrant region of flux as discussed in section 2.

7. Symmetric distribution of pinning centres

In this section we study, as an example, the case where a junction of length $\ell = 14.2$ contains three defects of length $d = 2$, and the distance between them is 2. The length was augmented, so that the defects keep the same width when we increase the number of defects, since we saw that width of the order $d = 2$ gives the possibility of fluxon trapping and increased maximum current when the defect is situated asymmetrically. We will study the phase distribution at $I = 0$ and try to extract information on the critical field values and magnetization. We find the following modes grouped according to flux content.

(i) *Modes 0, 0l, 0r, 0c.* In figure 12(a) we present the critical current plotted against the magnetic field for the modes

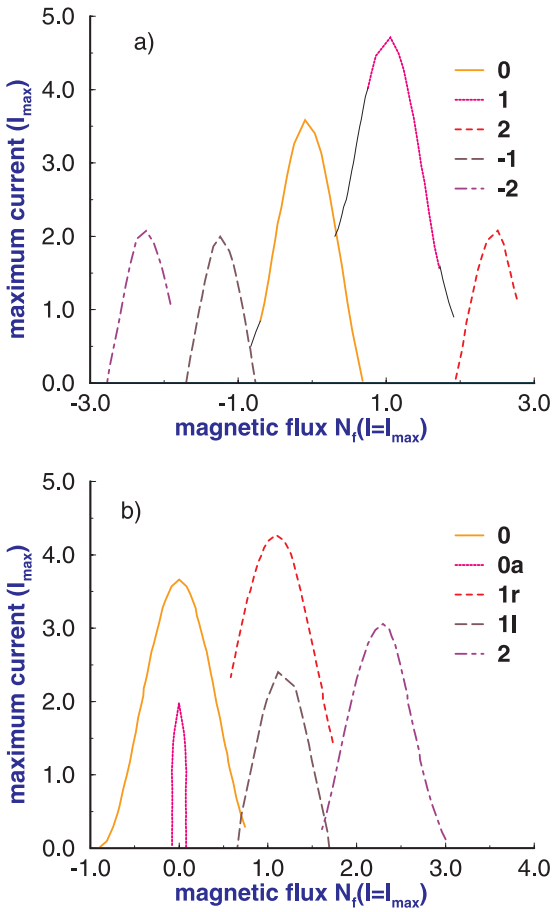

Figure 11. Critical current, I_c, plotted against the magnetic flux, N_f, at the maximum current for the different modes, for a junction of length $\ell = 10$: (a) for the asymmetric defect case and (b) for the two symmetric pinning centres of length $d = 2$.

with magnetic flux around zero (see figure 12(d)). This is indicated by the 0 symbol. There are four modes belonging in this category, which are stable. The solutions for mode 0 are similar to the homogeneous junction mode 0, with no flux trapping in the defects. The only difference is that the instability in the critical field occurs when the phase at one edge reaches a value which is smaller (due to pinning) than the corresponding value for the defect-free junction, which is $\phi(-\ell/2) < \pi$. The same is true for the two-defect case. Mode $0c$ has the maximum critical current $I_{max} = 5.08$ for $H = 0$. One antifluxon is trapped in the leftmost defect, one fluxon in the rightmost and the phase in the centre defect is constant. The trapping at the edge defects leads to a positive current distribution between them for this particular length and enlarges the maximum current. The same type of mode was not found for the two-defect case (with a shorter junction length), and we conclude that the extra defect along with the increased junction length stabilizes this solution. For mode $0l$ one fluxon is trapped in the left-hand defect where the phase changes about the value $\phi = \pi$. The antifluxon is distributed at the other two defects, where the phase is about the values $3\pi/2$ or $\pi/2$, and we have a cancellation of the positive and negative current density in this region. Similarly for mode $0r$ the fluxon is trapped in the right-hand defect, and the current is distributed

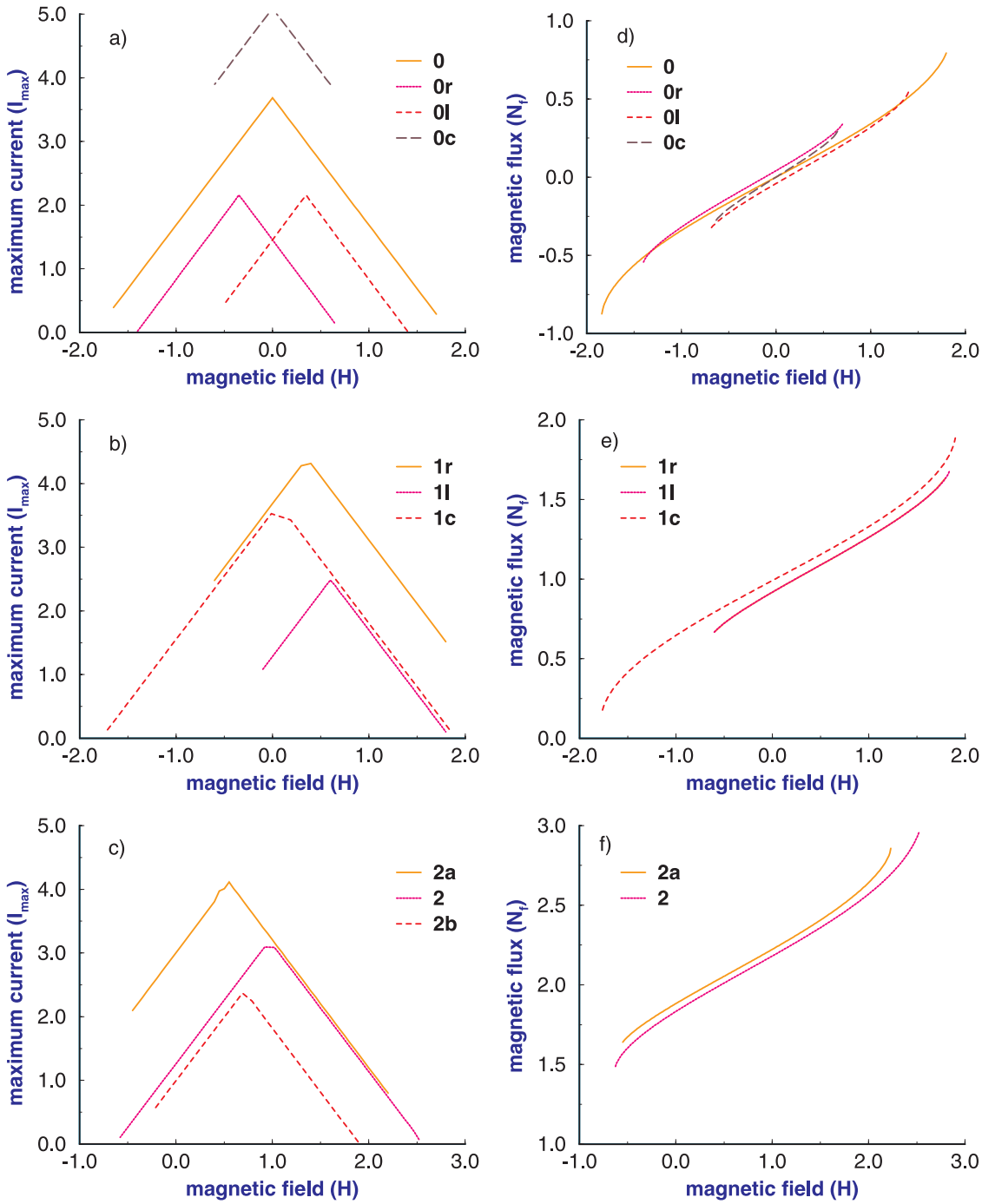

Figure 12. Critical current I_{max} plotted against the magnetic field, H, for the different modes: (a) 0, 0l, 0r, 0c, (b) 1r, 1l, 1c, and (c) 2, 2a, 2b for a junction of length $\ell = 14.2$ which contains three symmetric pinning centres of length $d = 2$. The corresponding magnetic fluxes are presented in (d), (e) and (f).

with opposite sign to the other two defects. These modes are similar to the 0a mode for the two-defect case.

(ii) *Modes 1l, 1c, 1r.* In figure 12(b) we see the maximum current plotted against the magnetic field for the modes with magnetic flux around $N_f = 1$ (see figure 12(e)). There are three modes with flux close to $N_f = 1$ each of which corresponds to the trapping of one fluxon in one defect. In mode 1c the fluxon is trapped in the centre defect. In mode 1l (1r) it is trapped in the left (right)-hand defect. Due to the symmetry, the lowest eigenvalue and the magnetic flux coincide for these two modes, but as we showed in the previous section, their critical currents are different, depending on the tunnelling current distribution in the region with no trapping. The 1r mode corresponds to a higher critical current.

(iii) *Modes 2, 2a, 2b.* In figure 12(c) we see the maximum current plotted against the magnetic field for the modes with magnetic flux around $N_f = 2$ (see figure 12(f)). Only mode 2 corresponds to stable solutions. There we have two fluxons trapped in the side defects. In mode 2a one fluxon is trapped in the right-hand defect, while in mode 2b this trapping occurs

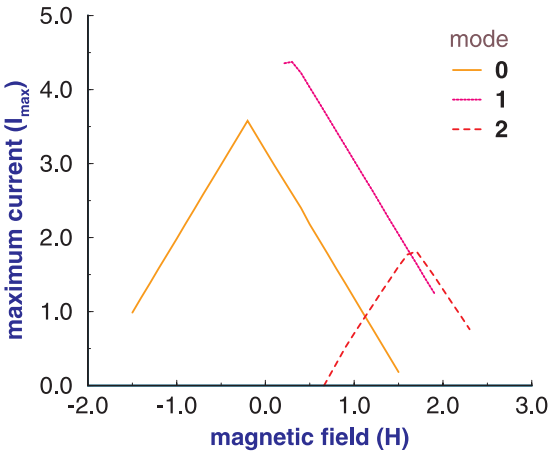

Figure 13. Inline critical current I_{max} plotted against the magnetic field, H, for modes 0, 1 and 2, for the junction with an asymmetric defect but smooth variation of the critical current density. $x_0 = 7.6$ and $\mu = 2$.

in the centre defect. We conclude that distributed pinning centres are more effective in trapping the vortex, and lead to an increased critical current. Some conclusions will continue to be valid for a larger number of defects where we keep the defect width and separation fixed. In such a case we also expect the results to change significantly when there is a periodic array of defects, where we expect higher fluxon modes to give the highest current peak [26].

8. Defect with a smooth variation of current density

Up to now we considered defects with abrupt changes in the local critical current density, and the question arises whether the abruptness of J_c variation is crucial in the significant change in I_{max} for the $n = 1$ mode. We will see that similar effects exist for smoother variation, where again fluxon pinning is an important feature. For this reason we chose a single defect at the junction centre with a smoothly varying critical current density given by

$$\tilde{J}_c(x) = \tanh^2\left[\frac{2}{\mu}(x - x_0)\right] \tag{9}$$

where the defect is centred at x_0, and the width is determined by μ. In figure 13 we show the results for the case $x_0 = 7.6$ and $\mu = 2$, which can be compared with the results of the asymmetric defect in figure 2(a). For the modes shown the curves are very similar and thus we see that the main results survive, since the defect strengths are similar. Of course there is a quantitative difference, but most of the stability criteria described earlier are still valid.

In figure 14 we consider the effect of the form of current input and compare the case of inline with overlap for a smooth defect situated at the centre of the junction i.e. $x_0 = 0$ with $\mu = 0.5$. In figure 14(a) we present I_{max} for inline boundary conditions, and we show only the -1, 0, 1 modes. The 0 mode is not influenced at all by the defect since all the phase variation is at the boundaries. There is a strong similarity with I_{max} for the 1 and -1 modes. The reason is that in these cases there is a trapped fluxon or antifluxon at the centre and at zero current and

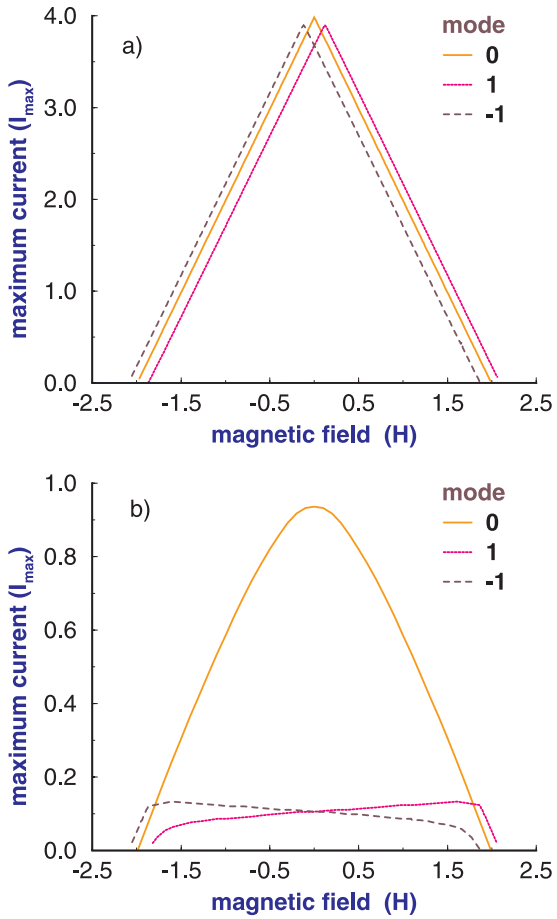

Figure 14. Critical current I_{max} plotted against the magnetic field, H, for the different modes, for (a) inline current and (b) overlap current, for the junction with a centred defect and smooth variation of the critical current density.

magnetic field the phase variation dies out at the boundaries. Thus when increasing the current at $H = 0$ towards I_{max} we have the same situation at the boundaries as for the 0 mode and the instability happens close to I_{max} values. Of course due to the pinning, the fluxon content is very different from the 0 mode. The -1 and 1 modes have an enhanced I_{max} and the small difference in I_{max} from the 0 mode is attributed to the small influence of the trapped fluxon on the boundaries. Let us remark that a similar situation was seen in figure 8(a) for the square well defect, when the defect position is at the centre for $H = 0$. By comparing, with figure 9, the H_{cl} and H_{cr} values we see a close agreement with the case of $j_d = 0$ in the defect. These results could change for a shorter junction or if we move the defect towards the edges (as seen in figure 8(a)).

For the same defect we also investigated the effect of the overlap current input, where the current is distributed along the whole junction. In figure 14(b) we present the maximum current per unit junction length plotted against the magnetic field, and it should be compared to the inline case in figure 14(a). We see a significant change for the -1 and 1 modes. Of course at $I = 0$ both current inputs give the same solution, but I_{max} is much smaller for the overlap boundary conditions. This is from the fact that due to the applied current, the fluxon is pushed against the pinning barrier until it is

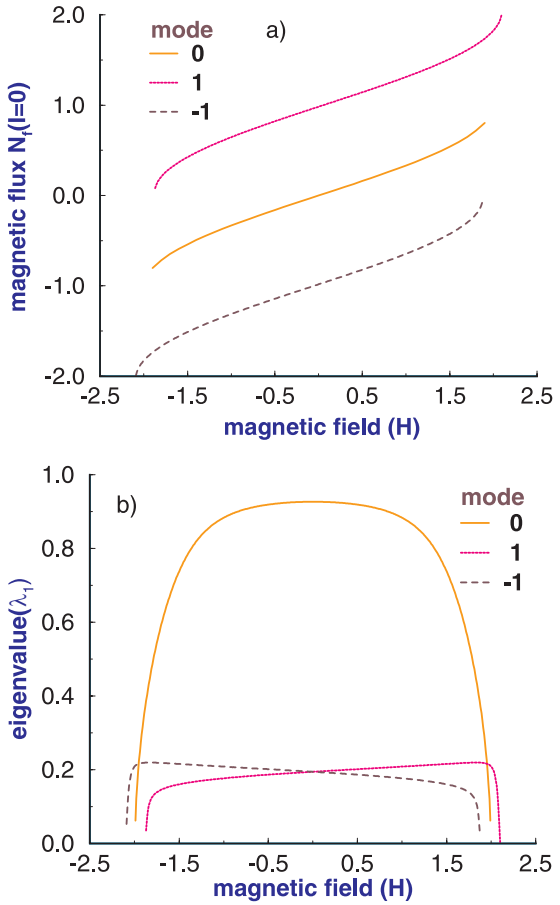

Figure 15. (a) Magnetic flux at zero current as a function of the external field for the same type of inhomogeneity as in figure 14. (b) The corresponding evolution of the lowest eigenvalue λ_1 for the different modes. At the end of each mode λ_1 vanishes.

overcome at the critical current. In the absence of an applied current the phase at the defect centre is $\phi(0) = \pi$, while the application of the current pushes the fluxon to the edge of the defect, which is taken to be near the point where the curvature of the defect critical current distribution changes sign. So in this case we can consider this maximum current as a measure of the pinning force.

In figure 15(a) we plot the magnetic flux N_f at zero current against the magnetic field H for the inline case. The lowest eigenvalues for the different modes against the magnetic field are seen in figure 15(b). For a homogeneous junction the 0 mode is the only stable state available at $H = 0$. However, in the problem we consider here, mode 1 (-1) exists and it is stable for $H = 0$ and corresponds to the localization of the soliton (antisoliton) in the inhomogeneity. For these modes we have a pinned flux at $H = 0$, with $\phi(0) = \pi$, and $\mathrm{d}\phi/\mathrm{d}x = 2$. In figure 16 we show the evolution of ϕ and $\mathrm{d}\phi/\mathrm{d}x$ for mode 1 as we change the magnetic field at $I = 0$. Near $H = -1.9$ the fluxon content is near zero and for $H < -1.9$ an instability sets in due to the depinning of the fluxon. This is because the slope at the pinned fluxon competes with the opposite slope that the external negative magnetic field tries to impose at the boundaries. At the other end the flux is equal to two, and the instability sets in when ϕ at the boundaries approaches π (or odd multiples). The range of H values for the 1 mode, when

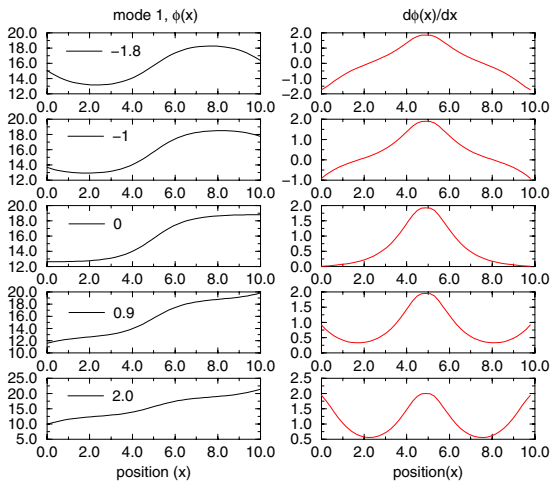

Figure 16. The evolution of $\phi(x)$ and $\mathrm{d}\phi(x)/\mathrm{d}x$ for mode 1 as we change the magnetic field at $I = 0$, for the same type of inhomogeneity as in figure 14. The numbers are H values.

the defect is at the centre, is significantly broadened and gives a corresponding range for the flux of two fluxons. Usually each mode has approximately one extra fluxon and, in particular, for the perfect junction it contains only one extra fluxon. This is because the defect is at the centre and far enough from the edges where the magnetic field is applied, and therefore even for negative fields there is no significant competition with the field at the defect centre. This is especially true when the distance of the defect from the edges is greater than $2\lambda_J$. When, however, the defect is near the edge the instability sets in before we cross to negative magnetic fields.

The maximum current I_{max} for mode 0 is greater than in modes 1,−1, but is reduced compared with the I_{max} for mode 0 in the homogeneous junction, in zero field. In [33] this reduction is approximated in an analytical calculation using a delta function for the defect potential, and it was found that $\Delta I_{max} = -\mu/2L \approx 0.02$. In [33] the authors arrived at the analytical result by minimizing the fluxon free energy, for the maximum overlap current against the magnetic field H for these modes, which is a good approximation of the numerical solution we consider here in the limit $L \gg 1$.

9. Conclusions

In many applications it is desirable to work in an extremum of the current for a region of the magnetic field. This can be achieved by the appropriate distribution of defects so that the negative lobes of the current distribution in the junction due to the fluxons are trapped in the defect with no contribution to the current. Of course if the defect is isolated (far from other defects or the edges) we expect a zero contribution to the current. Due to the effect of the applied current and magnetic field at the boundaries, in certain cases we can obtain positive current lobes outside the defect. In several cases in section 3 this was the reason for the increased current. Because the control of the magnetic field is very easy compared to other system parameters (like temperature, disorder, etc) the measurement of the effect of the magnetic field on junction behaviour provides a convenient probe for the

junction. The calculation of I_{max} can characterize the quality of the junction or verify the assumed distribution of defects when they are artificially produced. The spatial variation of the critical current density on low-T_c layered junctions, and high-T_c grain boundary junctions can be directly imaged with a spatial resolution of 1 μm using low-temperature scanning electron microscopy [34, 35]. Information on smaller scale inhomogeneities has to rely on the magnetic field dependence of the maximum tunnelling current I_{max}.

The purpose of this paper is the consideration of large defects in order to study the interaction between fluxons and defects and give estimates of the coercive field for pinning or depinning a fluxon from a defect. The region of consideration puts us far from the region of perturbation calculations and is amenable to direct experimental verification since it is easy to design a junction with the above characteristics. The defects strongly influence the low fluxon modes. At high magnetic fields, larger than the depinning field of a single fluxon, we expect only a minor effect and fluxon trapping. Of course for a large number of defects interesting behaviour can be obtained [24, 25]. The interaction between fluxons in the few-defect case also assists in overcoming coercive fields and untrapping fluxons. The results of two trapped fluxons in the two-defect case show that the fluxons are strongly coupled and one cannot consider an exponential interaction type potential between the fluxons. Also, the critical current in a long junction cannot be calculated as the Fourier transform of the spatial distribution of the critical current density $J_c(x)$, at least for weak magnetic fields. For strong magnetic fields, where we have the field uniformly penetrating the junction, as is the case for short junctions, we recover a diffraction like pattern.

In summary, we saw that the bounds of the different modes determined by the stability analysis depend on two factors: (i) the instability at the boundaries away from the defect when ϕ_x reaches its extremal values equal to ± 2 and (ii) the instability due to the pinning or depinning of a fluxon by the defect. If the junction is near one end then we saw that both criteria play a role in determining the instability, independently in different areas. In general, however, there will be coupling between defects and the edges (surface defects) especially in the case of multiple defects. Defects also introduce hysteresis phenomena which are weaker in the case of smooth defects. We also saw that due to fluxon trapping, in general, we see a re-entrant behaviour, i.e. there are regions of magnetic field for which there is both an upper and a lower bound on the maximum current. We also find that due to the pinning of magnetic flux from the defect there exist additional stable states in a large interval of the magnetic field. The abrupt change in the critical current density is not crucial for the trapping. Similar results are expected from smooth defects, with quantitative differences. The above results can be checked experimentally since it is easy to design a junction with a particular defect structure using masking techniques. In fact, a few parameters or characteristics could give, at least, partial information on the defect properties. In particular, the measurement of H_{cr} or H_{cl} can give some information on the defects near the edges. In addition, the measurement of the $I_{max}(H)$ diagram will give us information on the defect critical current density. Also, one can imagine the situation where we scan locally with an electron beam, thus affecting the local critical current, and observe the variation of the I_{max} as we increase the heating. Once a fluxon is trapped we can decrease the heating (or increase j_d) and observe the variation of I_{max}. Thus one can have pieces of information to put together in guessing the defect structure that might fit the whole I_{max} pattern. The extension to many defects requires considerable numerical work. It is hoped, however, that some of the stability criteria will still be useful.

Acknowledgments

One of us (NS) would like to acknowledge the ESF/FERLIN programme for partial support. Part of this work was carried out under grant PENED 2028 of the Greek Secretariat for Science and Research.

References

[1] Molshchakov V V, Kes P H and Brandt E H (ed) 2000 *Proc. Conf. Vortex Matter in Superconductors at Extreme Scales and Conditions, Physica* C **332** see several papers
[2] Barone A and Paterno G 1982 *Physics and Applications of the Josephson Effect* (New York: Wiley)
[3] Dimos D, Chaudhari P and Mannhart J 1995 *Phys. Rev.* B **41** 4038
[4] Sarnelli E, Chaudhari P and Lacey J 1993 *Appl. Phys. Lett.* **62** 777
[5] Gross R, Chaudhari P, Kawasaki M, Ketchen M B and Gupta A 1990 *Phys. Rev. Lett.* **57** 727
[6] Gross R, Chaudhari P, Dimos D, Gupta A and Kozen G 1990 *Phys. Rev. Lett.* **64** 228
[7] McCumber D E 1968 *J. Appl. Phys.* **39** 3113
[8] Miller D J, Talvacchio H, Buchholz D B and Chang R P H 1995 *Appl. Phys. Lett.* **66** 2561
[9] Ayache J, Torel A, Lesueur J and Dahmen U 1998 *J. Appl. Phys.* **84** 4921
[10] Fehrenbacher R, Geshkenbein V B and Blatter G 1992 *Phys. Rev.* B **45** 5450
[11] Oka T, Itoh Y, Yanagi Y, Tanaka H, Takashima S, Yamada Y and Mizutani U 1992 *Physica* C **200** 55
[12] Takagi A, Yamazaki T, Oka T, Yanagi Y, Itoh Y, Yoshikawa M, Yamada Y and Mizutani U 1995 *Physica* C **250** 222
[13] Wolf Th, Bornarel A-C, Kupfer H, Meier-Hirmer R and Obst B 1997 *Phys. Rev.* B **56** 6308
[14] Camerlingo C, Nappi C, Russo M, Testa G, Mezzetti E, Gerbaldo R, Ghigo G and Gozzelino L 2000 *Physica* C **332** 93
[15] Mezzetti E, Chiodoni A, Gerbaldo R, Ghigo G, Gozzelino L, Minetti B, Camerlingo C and Monaco A 2000 *Physica* C **332** 115
[16] Virokur M and Koshelev A E 1990 *JETP* **70** 547
[17] Kroger K, Smith L N and Jillie D W 1981 *Appl. Phys. Lett.* **39** 280
[18] van der Beek C J, Konczykowski M, Drost R J, Kes P H, Samoilov A V, Chikumoto N, Bouffard S and Feigel'man M V 2000 *Physica* C **332** 178
[19] Krasnov V M, Oboznov V A and Pedersen N F 1997 *Phys. Rev.* B **55** 14 486
[20] Ketchen M B 1991 *IEEE Trans. Magn.* **27** 2916
[21] Likharev K K and Semenov V K 1991 *IEEE Trans. Appl. Supercond.* **1** 3
[22] Kleinsasser A W, Mallison W H, Miller R E and Arnold G B 1995 *IEEE Trans. Appl. Supercond.* **5** 2735
[23] Reinisch G, Fernandez J C, Flytzanis N, Taki M and Pnevmatikos S 1988 *Phys. Rev.* B **38** 11 284
[24] Oboznov V A and Ustinov A V 1989 *Phys. Lett.* A **139** 481
[25] Larsen B H, Mygind J and Ustinov A V 1994 *Phys. Lett.* A **193** 359
[26] Itzler M A and Tinkham M 1995 *Phys. Rev.* B **51** 435

[27] Balents L and Simon S H 1995 *Phys. Rev.* B **51** 6515
[28] Caputo J-G, Flytzanis N, Gaididei Y, Stefanakis N and Vavalis E 2000 *Supercond. Sci. Technol.* **13** 423
[29] Owen C S and Scalapino D J 1967 *Phys. Rev.* **164** 538
[30] Chow T C, Chou H, Lai H G, Liu C C and Gou Y S 1995 *Physica* C **245** 143
[31] Yamashita T, Rinderer L, Nakajima K and Onodera Y 1974 *J. Low Temp. Phys.* **17** 191
[32] Yamashita T and Rinderer L 1975 *J. Low Temp. Phys.* **21** 153
[33] Filippov A T, Gal'pern Yu S, Boyadjiev T L and Puzynin I V 1987 *Phys. Lett.* A **120** 47
Filippov A T, Gal'pern Yu S, Boyadjiev T L and Puzynin I V 1975 *Phys. Lett.* A **21** 153
[34] Huebener R P 1988 *Adv. Electron. Electr. Phys.* **70** 1
[35] Gerdemann R, Husemann K D, Gross R, Alff L, Beck A, Elia B, Reuter W and Siegel M 1994 *J. Appl. Phys.* **76** 8005